Bioactive Materials 6 (2021) 1267–1282

Contents lists available at ScienceDirect

Bioactive Materials

journal homepage: www.sciencedirect.com/journal/bioactive-materials

A thermostability perspective on enhancing physicochemical and cytological characteristics of octacalcium phosphate by doping iron and strontium

Haishan Shi [a,b,c], Xiaoling Ye [b,c], Jing Zhang [b,c], Tingting Wu [e], Tao Yu [d], Changren Zhou [d], Jiandong Ye [b,c,*]

[a] School of Stomatology, Jinan University, Guangzhou, 510632, China
[b] National Engineering Research Center for Tissue Restoration and Reconstruction, South China University of Technology, Guangzhou, 510006, China
[c] School of Materials Science and Engineering, South China University of Technology, Guangzhou, 510640, China
[d] College of Chemistry and Materials Science, Jinan University, Guangzhou, 510632, China
[e] National Engineering Research Center for Healthcare Devices, Guangdong Institute of Medical Instruments, Guangdong Academy of Sciences, Guangzhou, 510500, China

ARTICLE INFO

Keywords:
Octacalcium phosphate
Thermostability
Iron
Strontium
Osteogenesis

ABSTRACT

Investigation of thermostability will lead the groundbreaking of unraveling the mechanism of influence of ion-doping on the properties of calcium phosphates. In this work, octacalcium phosphate (OCP), a metastable precursor of biological apatite, was used as a stability model for doping ions (Fe^{3+} and Sr^{2+}) with different ionic charges and radii. After treated under hot air at different temperatures (110–200 °C), the phase, morphology, structure, physicochemical properties, protein affinity, ions release, and cytological responses of the ion-doped OCPs were investigated comparatively. The results showed that the collapse of OCP crystals gradually occurred, accompanying with the dehydration of hydrated layers and the disintegration of plate-like crystals as the temperature increased. The collapsed crystals still retained the typical properties of OCP and the potential of conversion into hydroxyapatite. Compared to the undoped OCP, Fe-OCP, and Sr-OCP had lower and higher thermostability respectively, leading to different material surface properties and ions release. The adjusted thermostability of Fe-OCP and Sr-OCP significantly enhanced the adsorption of proteins (BSA and LSZ) and the cytological behavior (adhesion, spreading, proliferation, and osteogenic differentiation) of bone marrow mesenchymal stem cells to a varying extent under the synergistic effects of corresponding surface characteristics and early active ions release. This work paves the way for understanding the modification mechanism of calcium phosphates utilizing ion doping strategy and developing bioactive OCP-based materials for tissue repair.

1. Introduction

Based on the understanding of biological apatite of hard tissues, numerous trace elements, e.g. magnesium, zinc, iron, and strontium, have been utilized to improve the biological properties of calcium phosphate-based materials for tissue repair by doping methods owing to their distinct prominent functions [1–4]. Mg is beneficial to the adhesion of osteoblasts and the formation of new bone [3]. The introduction of Mg could inhibit the nucleation of growth of hydroxyapatite (HA) crystal, resulting in the lattice defects and the increments of the solubility, biodegradability, and osteoconductivity of HA [2,3]. As one of the key structural elements of many enzymes, Zn promotes the proliferation of osteoblasts, the synthesis of osseous proteins, and the formation of new bone in vivo [5]. Zn doping could promote the formation of poorly crystalized apatite-like phases, and osteogenic differentiation within a certain dose range [2,6,7]. Zn doping is also reported to endow calcium phosphates with antibacterial properties which were mainly derived from the release of Zn^{2+} [8,9]. Fe plays a crucial role in blood circulation, enhancing angiogenesis [10–12]. Fe incorporation could improve the stability and fracture toughness of calcium phosphates by incorporating Fe-containing ductile phase coupled with the matrix, and even endow them with unique magnetic properties [2,13,14]. Sr enhances the

* Corresponding author. National Engineering Research Center for Tissue Restoration and Reconstruction, South China University of Technology, Guangzhou, 510006, China.
E-mail address: jdye@scut.edu.cn (J. Ye).

https://doi.org/10.1016/j.bioactmat.2020.10.025
Received 25 August 2020; Received in revised form 14 October 2020; Accepted 25 October 2020
Available online 8 November 2020

proliferation and differentiation of pre-osteoblasts, meanwhile inhibited the formation and activity of osteoclasts [3,15]. Sr substitution could result in the lattice distortion of calcium phosphates, altering the crystallinity and biodegradability of the materials [15,16]. Consequently, these bioactive elements were introduced into calcium phosphates generally accompanied by the adjustments of their component, morphology, structure, physicochemical, and biological properties. Nevertheless, there were still few comparative studies concerning the impact of different ions on the physicochemical and biological properties of calcium phosphates, which could help further understand the distinctive changes brought about by ion doping.

We have previously discussed the influence of bioactive metal ions (Fe^{3+} and Sr^{2+}) with different ionic radii and charges on the formation, phase, and structure of octacalcium phosphate (OCP) comparatively [17]. The previous work highlighted the different replacements of complex Ca sites by Fe and Sr in OCP structure, but the cytological and biological evaluations were still limited. Beyond that, there are even no other research regarding the distinct influences of bioactive ion doping on the various properties of calcium phosphates, not to mention a detailed investigation from other perspectives. Herein, we attempted to understand the ionic doping strategy of calcium phosphates from a new perspective of stability, especially thermostability.

OCP, which is a key precursor of biological apatite, is an appropriate model to discuss the effect of ionic doping on the stability of calcium phosphates due to its controllable metastable characteristics [18,19]. OCP is easy to be converted into relatively stable apatite in vivo and in vitro, and that is, OCP-HA phase conversion occurs [18–21]. This conversion process, accompanied by the release of phosphate ions and the uptake of calcium ions, is generally recognized as an important reason for the excellent in vivo osteogenesis of OCP materials [18,22,23]. Important in this process are the changes in material surface properties: adsorption properties and protein-mineral interactions. At present, several studies were conducted to synthesize OCP samples with different degrees of conversion in these ways: 1) hot water incubation (60–80 °C) [24,25]; 2) fluorine-containing aqueous environment [24,26]; 3) organics or surfactants modification [25,27]; 4) high-temperature treatment (>700 °C) [25], etc. The post-treated OCP products generally had good protein affinity and osteogenic properties [24–29]. However, these rather drastic methods generally produced OCP products of extremely high degrees of conversion. There are still few studies reporting the protein affinity and biocompatibility of partially converted OCP materials obtained under milder conditions despite how sensitive OCP is to the surrounding environments. Moreover, except for fluorine ion, few studies paid attention to the conversion of OCP materials and the corresponding properties in the case of ionic doping. Suzuki and his coworkers improved the bioactivity of OCP-based materials by several milder methods (e.g. sterilized by heating at 120 °C) and studied the stability of the materials [6,18,30–32]. However, the influencing mechanisms of mild low-temperature treatment (e.g. at around 110–200 °C) on the stability of OCP materials modified with different bioactive ions remain unclear. Furthermore, the effect of the mild methods on the structural properties and ions release behaviors of OCP materials as well as subsequent biological responses still needed to be further unraveled in detail. Besides, it could be an effective way of using mild methods to further enhance the bioactivity of ion doped OCP materials by regulating the corresponding conversion degrees.

In this study, we comparatively introduced iron and strontium with different ionic radii and changes into OCP structure to regulate the physicochemical and biological properties of these materials by heat treatment at low temperatures (around 110–200 °C) under air. The hypothesis was that the heat treatment could mediate the protein affinity and biological responses of ion doped OCPs to varying extent owing to their different thermostability. The mechanism behind the relationship between the thermostability and the performances of OCP doped with distinct ions was unraveled based on the analysis of the phase, morphology, structure, physicochemical properties, ions release behaviors, and cytological responses of OCP materials treated at different temperature. This study can help to understand the roles of bioactive ions in the modification of calcium phosphates in vitro and in vivo, and to develop OCP-based biomaterials for tissue repair.

2. Experimental

2.1. Preparation procedure

OCP sample was synthesized by a homogeneous precipitation method as described in our previous work [17]. Briefly, a mixed solution containing 20 mM $Ca(CH_3COO)_2$, 15 mM $NH_4H_2PO_4$, and 50 mM CO $(NH_2)_2$ (carbamide) was gently stirred at 25 °C for 5 min and then vigorously stirred at 90 °C for 2 h. Subsequently, a white precipitate was collected, washed, centrifuged, and air-dried at 60 °C for 24 h. Fe $(NO_3)_3 \bullet 9H_2O$ and $Sr(CH_3COO)_2$ were used to synthesize iron- and strontium-doped OCPs (Fe-OCP and Sr-OCP), respectively. The Fe/(Fe+Ca) and Sr/(Sr+Ca) both were 5 mol.%. These synthetic samples were treated under hot air at 110, 130, 150, 170, and 190 °C for 2 h, respectively. The untreated samples of undoped OCP, Fe-OCP, and Sr-OCP were respectively employed as the corresponding controls. All the used chemicals were analytical reagents (purity >99.0%) and purchased from Sinopharm (China).

2.2. Characterization

The weight change of the samples by heat treatment was measured by a simultaneous thermal analyzer (STA449C, Netzsch, Germany) at a heating rate of 5 °C/min. The phase of the samples was identified by X-ray diffraction (XRD; X'Pert PRO, PANalytical, Netherlands) using CuKα radiation ($\lambda = 1.5418$ Å, 40 kV, 40 mA) at a step size of 0.033°. Fourier-transform infrared spectroscopy (FTIR) analysis was performed by a spectrometer (Vector 33-MIR, Brukev Optik, Germany) using samples in the form of pellets formed with spectroscopic grade potassium bromide (Sigma-Aldrich, USA). The morphology of the samples was observed by a field emission scanning electron microscope (FESEM; Nova NanoSEM 430, FEI, USA) at an accelerating voltage of 15 kV. The samples were spray coated with platinum before the observation. The zeta potential of the samples was measured by Zetasizer Nano ZS (Malvern, UK) after 30 min of ultrasonic dispersion in 10 mM potassium chloride solution at a particle concentration of 0.5 mg/mL. The specific surface of the samples was examined by N_2 adsorption-desorption porosimetry using a surface area analyzer (Nova 4000e, Quantachrome Instruments, USA).

2.3. Protein adsorption evaluation

Bovine serum albumin (BSA; Sigma Aldrich, USA) and lysozyme (LSZ; Sigma Aldrich, USA) were dissolved in phosphate buffer solution (PBS; 10 mM, pH 7.4, Toscience, China) at an initial concentration of 1 mg/mL. Afterward, OCP particles were immersed in the protein solutions at a concentration of 10 mg/mL at 37 °C for 3 h. The supernatants were collected by centrifugation at a speed of 13000 rpm after immersion. The concentration of proteins in the supernatants was tested by a BCA kit (Pierce BCA Protein Assay Kit, Thermo Scientific, USA). The absorbance was read at 562 nm by a microplate reader (Varioskan Flash Multimode Reader, Thermo Scientific, USA).

2.4. Cell culture

The mouse bone marrow mesenchymal stem cells (mBMSCs; CRL-12424, ATCC, USA) were maintained in culture flasks in a cell incubator at 37 °C (5% CO_2 atmosphere, 95% relative humidity). High-glucose Dulbecco's Modified Eagle's Medium (H-DMEM; Gibco, USA) with 10 vol% fetal bovine serum (FBS; Gibco, USA) was applied for the cell culture and replenished every other day. The cells were detached by 0.25% trypsin/EDTA (Gibco, USA) and used for the following seeding,

attachment, viability, proliferation, and differentiation assays. The cells at population of 4–6 passages were used in these experiments.

2.5. Cell seeding, attachment, viability, and proliferation

The OCP samples were sterilized by Co60 gamma radiation. Cells were directly seeded onto the culture plates at a density of 2×10^4 cells/cm^2. The culture media were refreshed with OCP-particles-containing media (1 mg/mL) after cell adhesion and this moment was set as the initial culture time. After cultured for 24 h, the cells were rinsed with PBS thrice and fixed with 4 vol% formaldehyde solution for 4 h. The fixed cells were dehydrated with a graded series of ethanol (30, 50, 60, 70, 80, 90, 95 and 100 vol%) and air-dried at room temperature for 24 h. The attachment and morphology of cells were observed by the FESEM.

Cells were cultured with OCP particles at a density of 5×10^3 cells/cm^2. After cultured for 3 days, the cells were rinsed with PBS thrice and double-stained with Calcein-AM (Biotium, USA) and propidium iodide (Biotium, USA) following the instructions. The fluorescence images of cells were acquired by an inverted fluorescence microscope (Eclipsc Ti–U, Nikon, Japan) equipped with a digital camera (40FL Axioskop, Zeiss, Germany). Quantitative cell viability was measured by a Cell Counting Kit-8 (CCK-8; Dojindo, Japan) assay. After cultured with OCP particles for 1, 3, and 5 days, the cells were incubated with the CCK-8 working solution at 37 °C for 1 h. Afterward, the absorbance of the supernatants was read at 450 nm by the microplate reader.

2.6. Alkaline phosphatase (ALP) activity test

Cells were cultured with OCP particles at a density of 5×10^4 cells/cm^2. The cells were cultured in the osteogenic medium which was supplemented with 10 mM sodium β-glycerophosphate (Merck Millipore, USA), 100 nM dexamethasone (Sigma Aldrich, USA) and 50 mg/L ascorbic acid (Sigma Aldrich, USA). The medium was refreshed every other day. After cultured with OCP particles for 7, 10 and 14 days, the cells were gently rinsed by cold PBS thrice and lysed by 10 mM Tris-HCl solution (pH 7.4) containing 500 μM $MgCl_2$ and 0.1 vol% Triton X-100 at 4 °C for 1 h. The supernatants were collected by sonication and centrifugation at 4 °C. The total protein content of the supernatants was tested by the BCA kit. ALP activity was measured by colorimetry at pH 10.4 in a glycine buffer containing 100 mM glycine, 1 mM $MgCl_2$, 1 mM $ZnCl_2$, and 5 mM *para*-nitrophenyl phosphate (*p*-NPP, Sigma Aldrich, USA). The absorbance was read at 410 nm by the plate reader. The ALP activity was normalized using the total protein contents.

2.7. Real-time qPCR (RT-qPCR)

Gene expression was quantitatively analyzed by the RT-qPCR method. For adhesion-related gene expression: after cultured with OCP particles at a density of 2×10^4 cells/cm^2 for 24 h, cells were lysed to isolate the total RNA by HiPure Total RNA Micro Kit (Magen, China). Afterward, the cDNA was yielded by the iScript cDNA Synthesis Kit (Bio-Rad, USA) and subjected to the qPCR test. The mRNA expressions of integrin α5 and β1 were measured, while β-actin was used as the housekeeper gene. The qPCR analysis was conducted by SYBR green assay (iQTM SYBR Green Supermix, Bio-Rad, USA). The gene expressions were calculated by *Equation* 1, where *Ct* represents the cycle number when an arbitrarily placed threshold was reached.

$$\text{Gene expression} = 2^{\text{Control group } (Ct_{\text{target gene}} - Ct_{\text{housekeeper gene}}) - \text{Sample group } (Ct_{\text{target gene}} - Ct_{\text{housekeeper gene}})} \quad (1)$$

For osteogenesis-related gene expression: after cultured with OCP particles in the osteogenic media at a density of 2×10^4 cells/cm^2 for 7 and 14 days, the qPCR test was performed to examine the mRNA expressions of Runx2, collagen 1 (Col1), and osteocalcin (OCN). Glyceraldehydes-3-phosphate dehydrogenase (GAPDH) was employed as the housekeeper gene. The forward and reverse primer sequences are listed in Table 1.

2.8. Immunofluorescence microscopy

Cells were cultured with OCP particles at a density of 2.5×10^4 cells/cm^2. After cultured for 24 h, the cells were rinsed with PBS thrice and then fixed by 4 vol% formaldehyde solution for 20 min. The fixed cells were permeabilized with 0.1 vol% Triton X-100 (Sigma Aldrich, USA) for 10 min. The actin microfilaments and nuclei of cells were stained by phalloidin (AAT Bioquest, USA) and 4′,6-Diamidino-2-Phenylindole (DAPI; Beyotime, China). Focal adhesion (FA) contact was stained by vinculin using an anti-vinculin antibody (Abcam, USA) and Cy3-conjugated Affinipure Goat Anti-Rabbit IgG (H+L) (Protein Tech Group, USA). Integrin α5 were stained by anti-integrin α5 antibody (Abcam, USA) and Cy3-conjugated Affinipure Goat Anti-Rabbit IgG (H+L) (Protein Tech Group, USA). The cytoskeleton arrangement, FA contact, and integrin α5 distribution of cells were analyzed by a confocal laser scanning microscope (CLSM; TCS SP5, Leica Microsystems, Germany).

2.9. Ions release test

OCP particles were immersed in culture media at a concentration of 1 mg/mL and incubated in a shaker (770R, APlus, USA) at 37 °C. The media were refreshed every other day and collected at the predetermined intervals. The ionic concentrations of calcium, phosphate, iron, and strontium in the well-digested medium was tested by an inductively coupled plasma atomic emission spectroscope (ICP-AES; Optima 5300DV, PerkinElmer, USA).

2.10. Statistical analysis

The proteins adsorption and cell experiments were repeated four times. The tests of zeta potential and the ions release test were repeated five and three times, respectively. Quantitative data were averaged and expressed as the standard deviation to the mean. Statistical analyses were performed using a one-way analysis of variance (one-way ANOVA). A comparison between two means was made using the Tukey's test with statistical significance set at $P < 0.05$.

3. Results and discussion

3.1. Thermostability, phase, morphology, and structure of ion doped OCPs after treatment

Fig. 1 gives the TG-DTG plots of undoped OCP, Fe-OCP, and Sr-OCP. Thermal weightlessness was detected in all the samples within a range of temperatures from 40 °C to 280 °C. The weight loss of both Fe-OCP and

Table 1
Validated primer sequences for real-time PCR.

Gene	Direction	Sequence (5′-3′)
Integrin α5	Forward	TGCAGTGGTTCGGAGCAAC
	Reverse	TTTTCTGTGCGCCAGCTATAC
Integrin β1	Forward	ATCATGCAGGTTGCGGTTTG
	Reverse	GGTGACATTGTCCATCATTGGGTA
β-actin	Forward	TGACAGGATGCAGAAG GAGA
	Reverse	GCTGGAAGGTGGACAGTGAG
Runx2	Forward	CACTGGCGGTGCAACAAGA
	Reverse	TTTCATAACAGCGGAGGCATTTC
Col1	Forward	ATGCCGCGACCTCAAGATG
	Reverse	TGAGGCACAGACGGCTGAGTA
OCN	Forward	AGCAGCTTGGCCCAGACCTA
	Reverse	TAGCGCCGGAGTCTGTTCACTAC
GAPDH	Forward	TGTGTCCGTCGTGGATCTGA
	Reverse	TTGCTGTTGAAGTCGCAGGAG

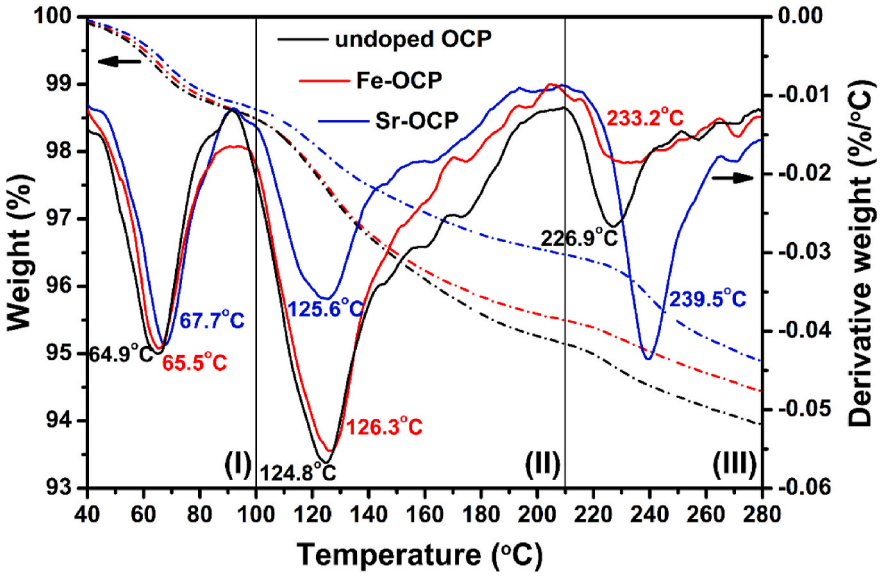

Fig. 1. The thermostability of OCP was affected by the ionic doping. TG-DTG plots of undoped OCP, Fe-OCP, and Sr-OCP.

Sr-OCP samples was lower than that of undoped OCP. Besides, the DTG peaks of Fe-OCP and Sr-OCP shifted to the right (higher temperature) compared to that of undoped OCP. It was reported that OCP crystals could lose three of five structural water molecules and finally convert into poorly crystallized apatite during the thermal process, which included two steps: the first step (<100 °C) is a reversible process, where dehydration of one water molecule led to a slight shrinkage of OCP crystals; the second step (130–150 °C) is an irreversible process, where a further dehydration of two water molecules induced the gradual phase conversion of OCP into poorly crystallized apatite [33,34]. The thermal procedure would involve chemical reactions as follows:

$$Ca_8H_2(PO_4)_6{\cdot}5H_2O \rightarrow Ca_8H_2(PO_4)_6{\cdot}4H_2O + H_2O\uparrow\ (<100^oC) \quad (2)$$

$$Ca_8H_2(PO_4)_6{\cdot}4H_2O \rightarrow Ca_8H_2(PO_4)_6{\cdot}2H_2O + 2H_2O\uparrow\ (130\text{-}150^oC) \quad (3)$$

According to the thermal analysis, the weight loss process of OCP could be roughly divided into three stages: (I) 40–100 °C, first dehydration stage; (II) 100–210 °C, second dehydration stage; (III) 210–280 °C, phase conversion stage. In this regard, the second stage could even continue to 210 °C rather than in the range of 130-150 °C. During the third weight loss stage, a structural transformation (or arrangement) of the "water-free" dehydrated OCP gradually took place. Thermostability is generally determined by the residual weight of solid phases or the temperature at which a certain weight loss ratio reaches after heat treatment. According to the weight loss ratio of the samples at different temperature points from the TG curves, in order of best thermostability, it went: Sr-OCP, Fe-OCP, and undoped OCP. Moreover, the thermostable difference mainly occurred in the latter two irreversible stages. It was indirectly indicated that iron and strontium had been doped into the structure of OCP crystals on the basis of the previous work [17]. It is reported that Sr^{2+} incorporation can stabilize the metastable calcium phosphate phases (such as OCP) by performing first-principles calculations of substitutional Sr^{2+} defects in OCP [35]. From an experimental perspective, it provided evidence that the incorporation of moderate amount of Sr could stabilize the stability of OCP crystals to some extent. Hence, the incorporation of iron and strontium enhanced the thermostability of OCP crystals to some extent.

Fig. 2 shows the XRD patterns and FTIR spectra of undoped OCP, Fe-OCP, and Sr-OCP treated at different temperature. An exclusive phase of octacalcium phosphate (JCPDS PDF#26–1056) was detected for all the untreated samples which maintained their phases at 110 °C. As the temperature increased to 130 °C, a shoulder diffraction peak near $2\theta =$ 4.7° [face $(100)_{OCP}$], which was attributed to the face *(100)* of the dehydrated OCP structure, appeared in the diffraction patterns of all OCP samples. Meanwhile, the main specific diffraction peaks of OCP became weaker or even disappeared along with the appearance of apatite-like diffraction peaks. With the increment of temperature, the intensity of the diffraction peak of the face $(100)_{OCP}$ markedly decreased, whilst that of the shoulder peak gradually increased. At 190 °C, the peak of the face $(100)_{OCP}$ almost disappeared, and that of other lattice faces, such as *(-302)*, *(620)*, *(-421)* and *(700)*, also disappeared or broadened. By contrast, the intensity of the face $(002)_{OCP}$ was hardly altered or even enlarged by the heat treatment, and just a very slight shift to the peak position of the face (002) of HA (JCPDS PDF#09–0432) or enlargement of the diffraction peak of the face was detected for the samples treated at 190 °C (as marked by blue arrows in Fig. 2b). Specifically, at 170 °C, a more obvious phase change was found for Fe-OCP compared to that of undoped OCP. Conversely, Sr-OCP was more thermostable because of the greater intensity of the faces $(100)_{OCP}$ and $(700)_{OCP}$ compared to undoped OCP. The crystallite sizes of these samples were calculated based on the *Scherrer Equation* after pattern fitting (Fig. 2c). The heat treatment lowered the crystallite sizes of OCP crystals gradually in a temperature-dependent manner. Notable lattice contraction was also detected for the treated OCP crystals according to the refined results obtained by performing the Rietveld refinement using the structural model of OCP (ICSD #65347) (see Table S1). Smaller lattice parameters of the *a*- and *b*-axes as well as the unit cell volume of the treated OCP crystals were revealed compared to those of untreated crystals. The structural collapse and disintegration of these crystals were directly resulted from the dehydration process especially in the hydrated layers of OCP crystals.

From FTIR spectra, two sharp bands of PO_4^{3-} at 560 and 602 cm^{-1} were ascribed to crystalline calcium phosphate. The broad band at 860 cm^{-1} was attributed to the characteristic adsorption of HPO_4^{2-} in the hydrated layers of OCP crystals. Two bands at 962 and 1038 cm^{-1} were attributed to the P–O stretching vibration of PO_4^{3-}. A shoulder band at 1124 cm^{-1} belonged to HPO_4^{2-}. These main vibration peaks of PO_4^{3-} and HPO_4^{2-} groups were typical of the OCP structure [17]. The characteristic bands of all OCP samples were comparable with each other after heat treatment. That was, no obvious difference in structural characteristics of phosphate groups was detected among all OCP samples. Herein, the dehydration process slightly affected the apatite layers of OCP crystals, the structure of which is very similar to that of HA crystals. It was in accordance with the XRD results which indicated the structural

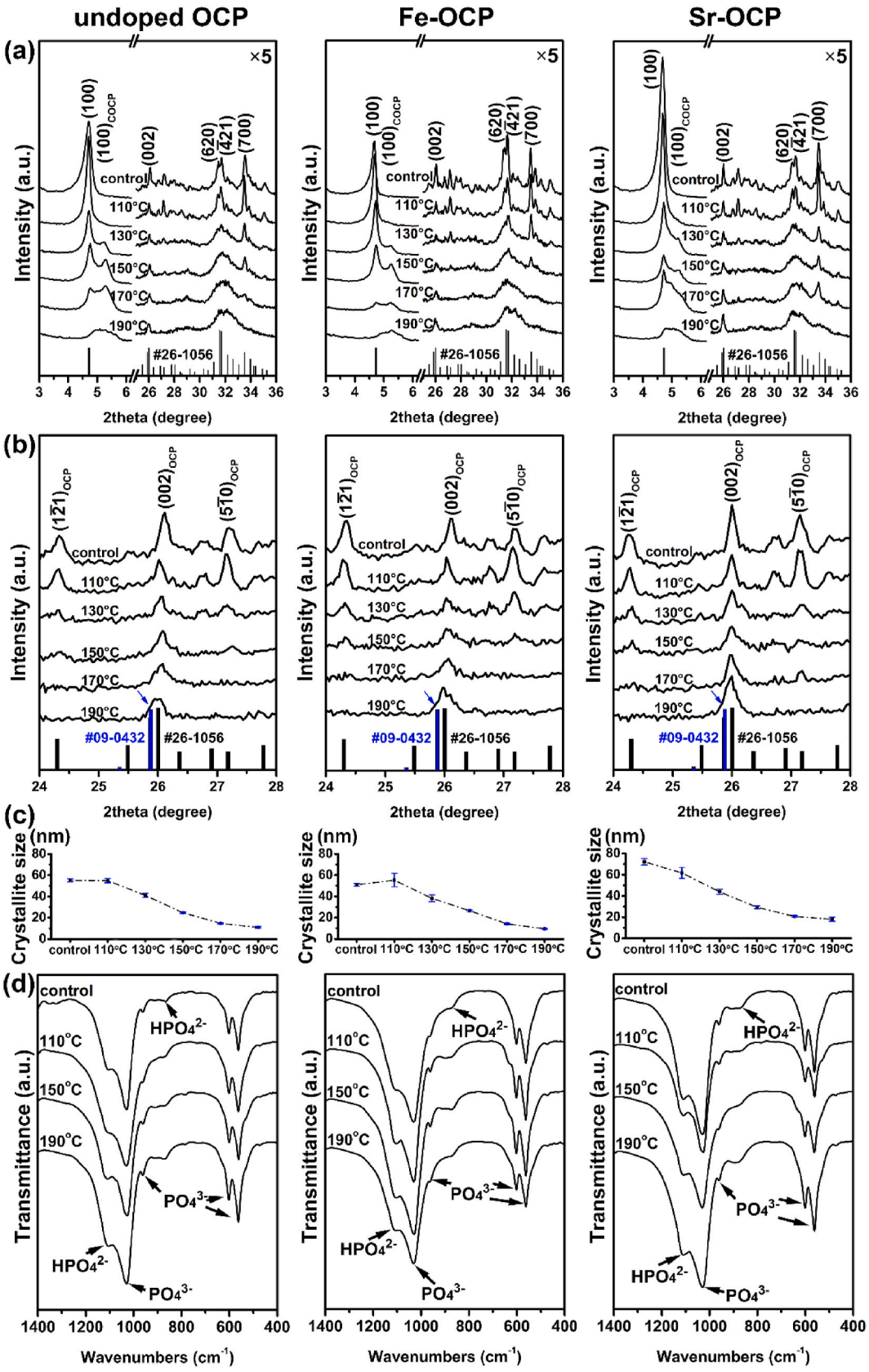

Fig. 2. Heat treatments significantly altered the phase components of OCP samples. XRD patterns (a, b), calculated crystallite sizes (c) and FTIR spectra (d) of undoped OCP, Fe-OCP, and Sr-OCP heat-treated at different temperatures.

rearrangement of the face $(002)_{OCP}$ to its structurally similar $(002)_{HA}$ along the *c*-axis [34,36]. In this regard, the dehydration was supposed to mainly occur in the hydrated layers of OCP crystal, leading to the structural changes of OCP and the formation of "collapsed OCP" [34]. The specific diffraction patterns of these collapsed OCP were close to that of apatite, marking a new stage where the structure was about to convert into that of HA. The XRD results also indicated a lower thermostability of Fe-OCP compared to that of undoped OCP, which was inconsistent with the TG analysis. In our previous work, nanosized ferric phosphates were deposited on the surface of Fe-OCP crystals. It was inferred that the ferric phosphate deposits had a very low weight loss ratio (or degree of dehydration), which would interfere the result of TG analysis and thus covered up the true thermostability of Fe-OCP to some extent. Sr-OCP remained a more complete characteristic of OCP structure, indicating the role of strontium as a stabilizer of OCP crystals. Therefore, the phase conversion of OCP was mainly derived from the dehydration in hydrated layers accompanied by slight changes of apatite layers at around 110–190 °C. In addition, the doping of iron or strontium notably altered the thermostability of OCP crystals.

Fig. 3 displays the SEM images of undoped OCP, Fe-OCP, and Sr-OCP treated at different temperature. All OCP crystals revealed typical plate-like feature. With the increment of temperature, these plates gradually disintegrated into smaller fragmentary crystals as a result of the dehydration process which was consistent with the XRD results. The appearance of all OCP crystals treated at 110 °C was similar to that of the untreated samples, accompanied by a few disintegrated crystals. As temperature increasing to 190 °C, the disintegration phenomenon of these crystals was extremely obvious. Specifically, the plate-like Fe-OCP

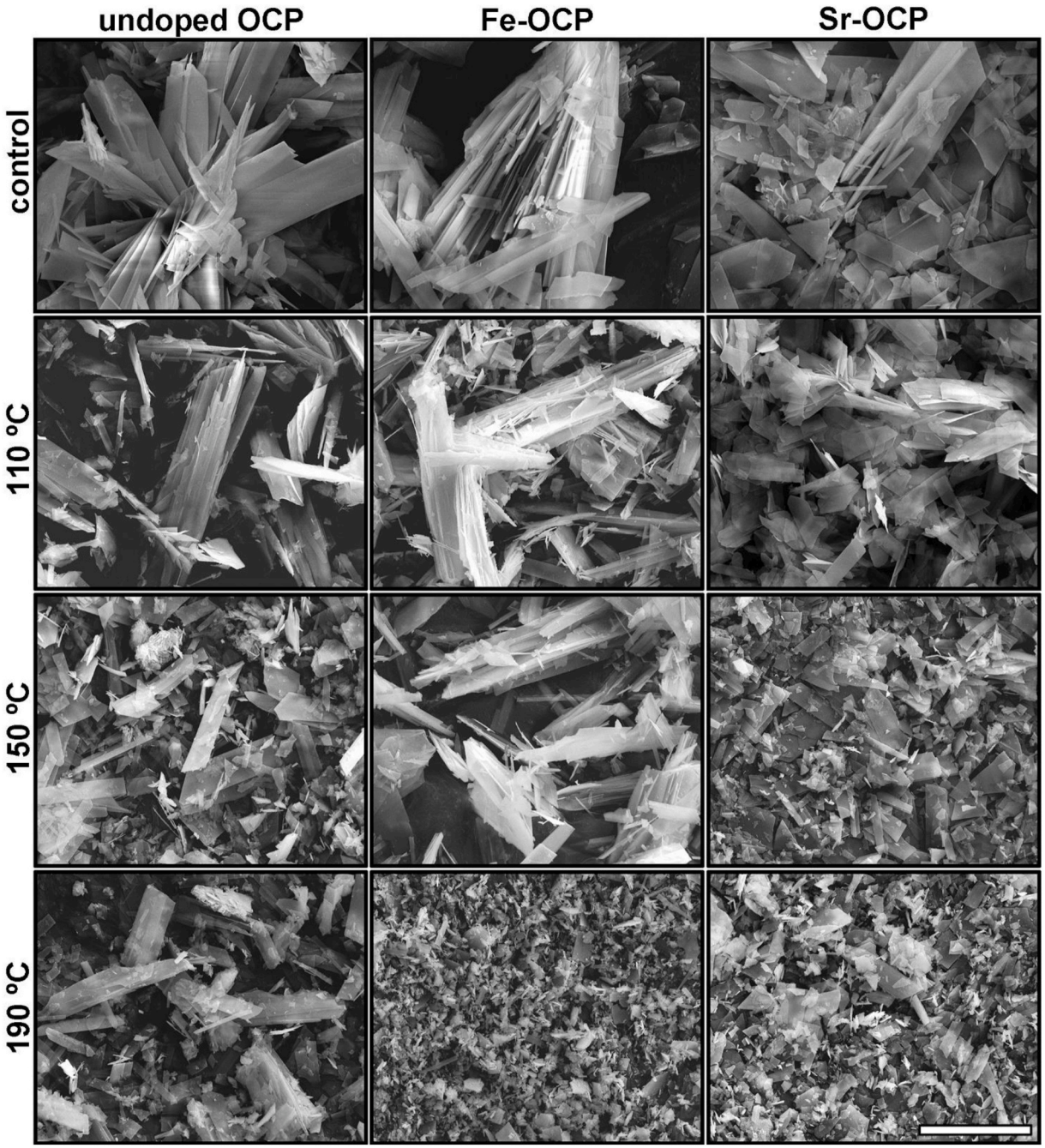

Fig. 3. Heat treatments significantly altered the morphology of OCP samples. SEM images of undoped OCP, Fe-OCP, and Sr-OCP heat-treated at different temperatures. Scale bar = 20 μm.

crystals almost completely converted into uniform fine crystals. By contrast, Sr-OCP crystals were relatively more stable and a certain amount of Sr-OCP plates was still observed. It was of indicative that incorporation of strontium improved the thermostability of OCP crystals whereas iron doping did the reverse, which was consistent with the results above.

3.2. Surface nature and protein adsorption of ion doped OCPs after treatment

Fig. 4 shows the surface zeta potentials, specific surface areas, and proteins (BSA and LSZ) adsorption behaviors of undoped OCP, Fe-OCP, and Sr-OCP treated at different temperature. Compared to undoped OCP (-9.38 ± 3.40 mV), Fe-OCP had a significantly more negative surface (-25.20 ± 3.21 mV), whilst Sr-OCP was weakly electronegative (-5.98 ± 2.89 mV). The electronegativity of undoped OCP and Fe-OCP gradually decreased with the increase of temperature, and that of Sr-OCP had no evident changes. The specific surface areas of all the samples gradually enlarged as the temperature increased. In comparison to undoped OCP and Fe-OCP, the specific surface area of Sr-OCP had a relatively smaller change. After the heat-treatment, an obviously enhanced adsorption behaviors of both proteins were determined for undoped OCP samples, which was not associated with the temperature; Fe-OCP samples had an improved BSA adsorption capacity without any influence of temperature, but a reduced LSZ adsorption performance in a temperature-dependent manner; there was no obvious difference of proteins adsorption between the untreated and the treated Sr-OCP samples.

Generally, the surface potential of biomaterials is one of the critical properties which are involved in direct interactions of bioprotein molecules and materials surface, especially the process where electrostatic interaction plays a major role [37,38]. Here, the surface of all OCP samples was negative in the simulated physiological environments, which could be beneficial for their cell response [39]. Moreover, the surface potential changes of these OCP samples were broadly in line with their corresponding thermostability. It was reported that Sr^{2+} mainly replaced the Ca^{2+} sites in the hydrated layers of OCP crystals, which could stabilize the layers and maintain a more complete crystal structure after dehydration of the layers [17,35]. In this regard, Sr-OCP could remain a certain structural reversibility. As resuspended in an aqueous solution, the hydrated layers vacancies resulted from Sr^{2+} occupancy would provide diffusion channels for the uptake of water molecules, maintaining relatively similar physicochemical properties of Sr-OCP after heat treatment. For Fe-OCP, Fe mainly replaced the Ca^{2+} sites in apatite layers in the form of Fe^{3+} and ferric hydroxo ions [$Fe(OH)_2^+$/$Fe(OH)^{2+}$] [17]. The dehydration could lead to the destruction of the hydrated layers of Fe-OCP, and the apatite layers of that were also somehow destroyed because of the instability of ferric hydroxo ions. Thus, Fe-OCP was less stable than undoped OCP. The report has suggested that surface potential of OCP crystals is closely related to their solubility: in the aqueous solution, Ca^{2+} concentration increased with the increase of solubility of OCP, resulting in a wholly enlargement of zeta potential [40]. Hence, the heat treatment improved the solubility of undoped OCP to some extent accompanied with a slight increase of its zeta potential;

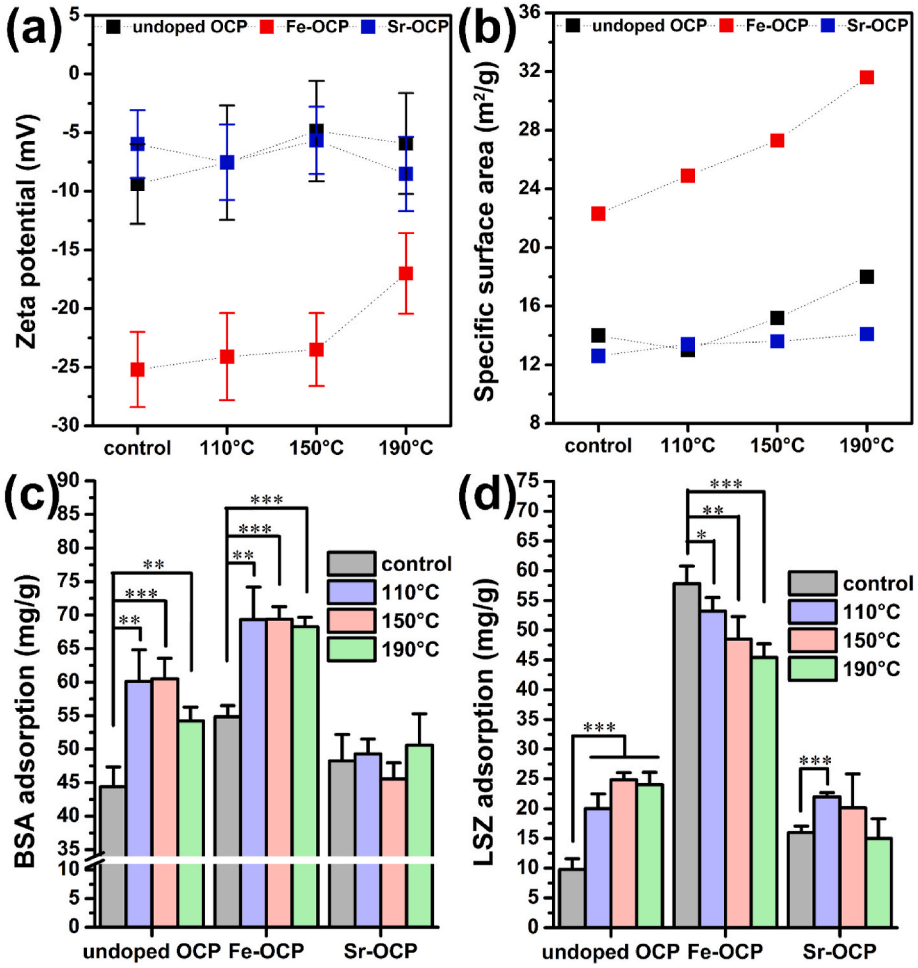

Fig. 4. Heat treatments significantly altered the surface characteristics and protein behaviors of OCP samples. Surface potentials (a), specific surface areas (c), and proteins adsorption (c, d) on undoped OCP, Fe-OCP, and Sr-OCP heat-treated at different temperatures.

Sr-OCP was more stable and its surface potential had little change; Fe-OCP had a greater solubility and released a higher-dose Ca^{2+} after the treatment, generating a gradual decrease of surface electronegativity.

The increased specific surface of OCP samples was a direct result of crystal disintegration generating new fresh surface. Fe-OCP and undoped OCP were more sensitive to the heat treatment in the light of their rapidly rising surface area; by contrast, Sr-OCP was more stable confirmed by its smaller change of surface area. The results provided direct evidence for the SEM observation. It was noted that, Fe-OCP group had higher specific surface areas than other groups, which was probably derived from the presence of nanosized ferric phosphate deposits. The altered surface characteristics of OCP samples by heat treatment should further affect the protein adsorption behaviors of the materials. BSA and LSZ were selected as the model proteins for their distinctly different electrostatic properties. BSA is a flexible globular macromolecule (Mw ~66 kDa) with an isoelectric point of 4.7 [41]. BSA adsorption is generally driven by its conformational change and the electrostatic interaction of surface-molecule [41]. For undoped OCP, compared to the untreated samples, the preponderant BSA adsorption on the heat-treated samples could be mainly due to the lower electrostatic repulsions of surface-BSA and the conformation changes of BSA molecules on the surface based on the result of specific surface area normalization (see Fig. S1); by contrast, the enhanced BSA adsorption of Fe-OCP samples came more from the contribution of the significantly larger specific surface area after treatment. LSZ was a smaller rigid molecule (Mw ~14 kDa) with an isoelectric point of 11.1. LSZ adsorption mainly comes from the contributions of electrostatic force [37]. LSZ was positively charged and preferred adsorbing on the negative surface in the environment. The most electronegative Fe-OCP had the largest LSZ adsorption among all OCP samples (Figs. 4d and S1). Moreover, the behavior of LSZ adsorption on the heat-treated Fe-OCP had a direct relationship with the significant changes of surface electronegativity as mentioned above. Specifically, a passivation behavior in the proteins' adsorption of the heat-treated Sr-OCP was detected, which could be derived from the higher thermostability and the more stable surface of Sr-OCP compared to undoped OCP and Fe-OCP.

3.3. Cell responses of ion doped OCPs after treatment

Fig. 5 demonstrates the SEM images of mBMSCs adhered on the heat-treated undoped OCP, Fe-OCP, and Sr-OCP after co-cultured for 24 h. All OCP samples revealed good cellular affinity. The cells contacted with these samples, adhered and spread well on them. Fig. 6 further gives the immunofluorescence images of DAPI, F-actin and focal adhesion (FA) of mBMSCs after co-cultured with heat-treated undoped OCP, Fe-OCP, and Sr-OCP for 24 h, respectively. The cells in both undoped OCP and Fe-OCP groups showed good spreading morphology. Meanwhile, the heat-treated samples in the two groups had a promotion effect in vinculin expression of mBMSCs compared to their control samples. All Sr-OCP samples also had a good cellular affinity, however, a slight weaker vinculin expression was observed in their heat-treated samples than that in the control. ImageJ 1.51r software (National Institutes of Health, NIH; USA) was used to quantitatively analyze cellular areas and FA areas of cells adhered on the samples. The cells on the heat-treated undoped OCP and Fe-OCP samples had comparable spreading areas and higher FA fluorescence intensity compared with the corresponding controls. By contrast, greater spreading areas and lower FA fluorescence intensity were determined for cells on the heat-treated Sr-OCP samples than those on the control. Herein, the treatment affected cellular affinity and adhesion of OCP samples. In addition, compared to the control, both the heat-treated undoped OCP and Fe-OCP samples up-regulated the vinculin expression of mBMSCs, while the heat-treated Sr-OCP down-regulated this expression to some extent.

To further investigate the influence of heat treatment on the cellular adhesion behaviors on OCP samples, the integrin α5β1 mRNA expression level of mBMSCs on OCP samples was tested by the RT-qPCR method and immunofluorescence staining, as shown in Fig. 7. Compared to the control, both the heat-treated undoped OCP and Fe-OCP samples

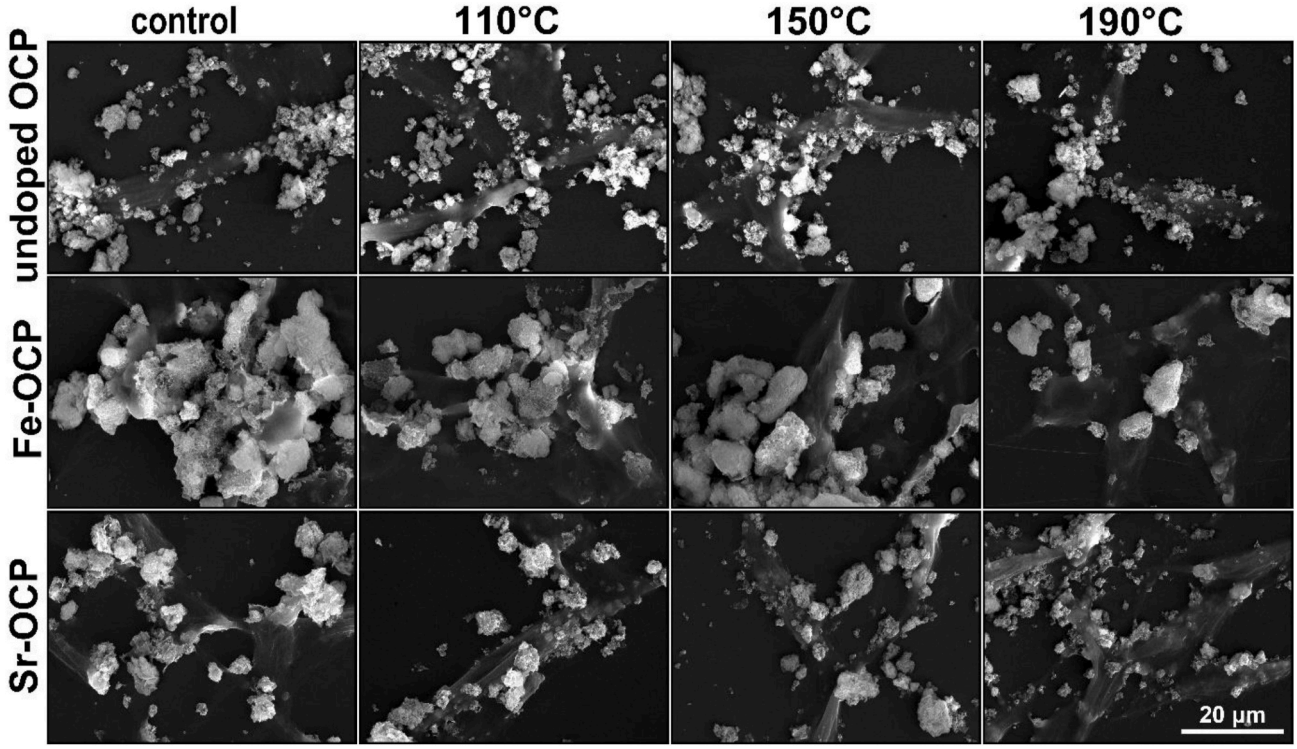

Fig. 5. The heat-treated OCP samples showed good cell affinity. Cells had good spreading state accompanied with decoration by small mineral particles derived from the evolution of OCP crystals. SEM images of BMSCs adhered on heat-treated undoped OCP, Fe-OCP, and Sr-OCP after co-cultured for 24 h, respectively. Scale bar = 20 μm.

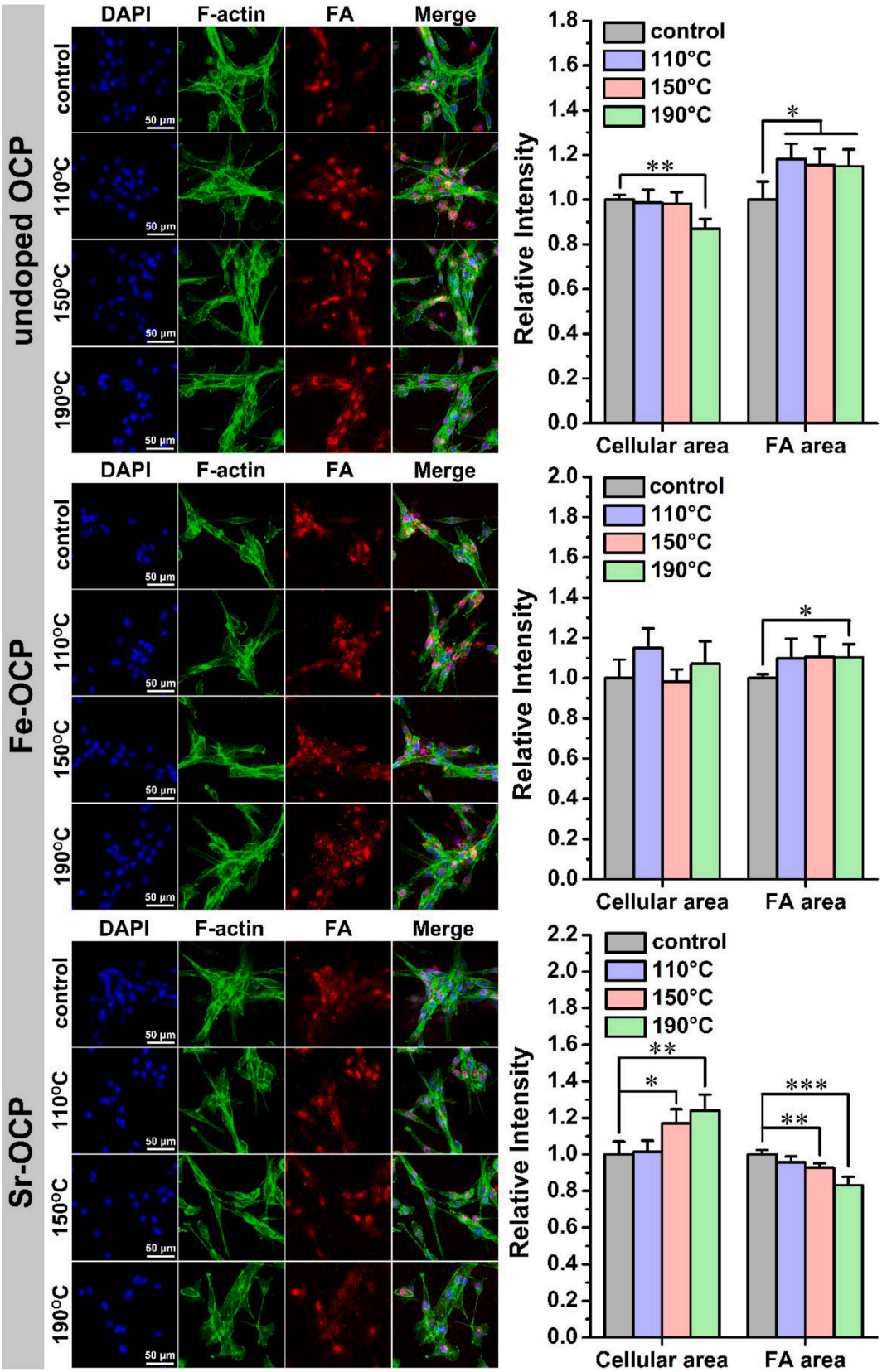

Fig. 6. Heat treatments significantly altered the cell adhesion performance of OCP samples. Immunofluorescence images of DAPI (blue), F-actin (green), focal adhesion (FA, red), and their merged images of BMSCs after co-cultured with heat-treated undoped OCP, Fe-OCP, and Sr-OCP for 24 h, respectively. Scale bar = 50 μm. Spreading of BMSCs was quantified by measuring cellular areas and FA areas of more than 200 cells. Data were presented as mean ± S.D., $n = 4$. * Heat-treated samples compared with the control sample. *$P < 0.05$, **$P < 0.01$, ***$P < 0.001$. (For interpretation of the references to color in this figure legend, the reader is referred to the Web version of this article.)

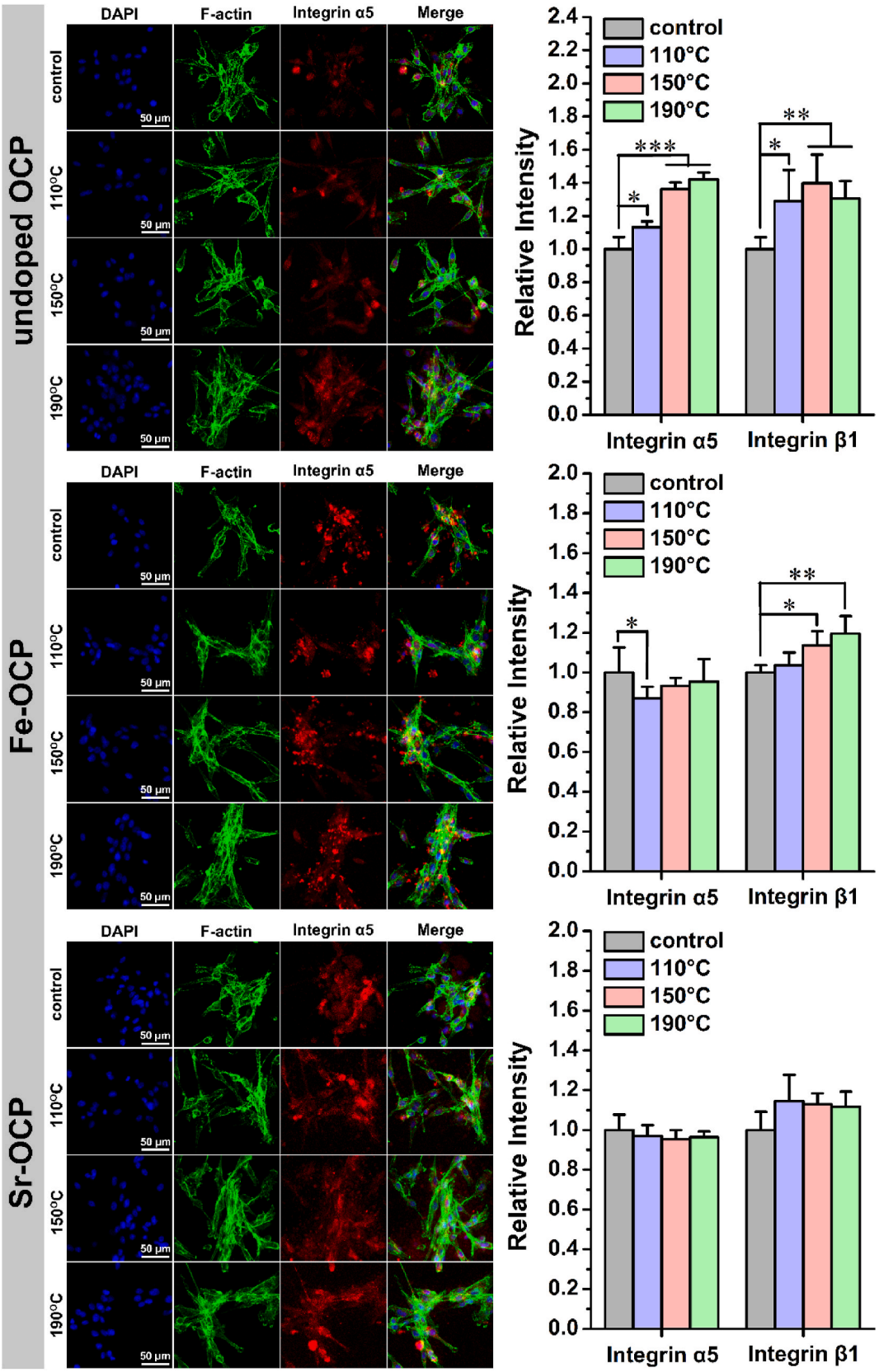

Fig. 7. The improved adhesion-related gene expression of BMSCs was determined as cultured with the heat-treated OCP samples. Immunofluorescence images of DAPI (blue), F-actin (green), integrin α5 (red), and their merged images, as well as cellular adhesion-related gene expression of BMSCs after co-cultured with heat-treated undoped OCP, Fe-OCP, and Sr-OCP for 24 h, respectively. Scale bar = 50 μm. Data were presented as mean ± S.D., $n = 4$. * Heat-treated samples compared with the control sample. *$P < 0.05$, **$P < 0.01$, ***$P < 0.001$. (For interpretation of the references to color in this figure legend, the reader is referred to the Web version of this article.)

notably promoted the mRNA expression of integrin α5β1 in a temperature-dependent manner; the mRNA expression of integrin α5β1 on the heat-treated Sr-OCP had no significant difference. From immunofluorescence staining images, the fluorescence intensity of integrin α5 of mBMSCs on both the heat-treated undoped OCP and Fe-OCP samples was significantly higher than that on the control; the heat-treated Sr-OCP samples showed a comparable immunofluorescence staining result with the corresponding control. The immunofluorescence observation was in accordance with the mRNA expression of integrin above. Hence, after heat-treatment, undoped OCP and Fe-OCP samples markedly up-regulated cellular adhesion related integrin gene expression, whereas Sr-OCP samples made no difference. According to the results above, heat-treatment altered the surface physicochemical properties of OCP samples, which could activate corresponding surface layers to some

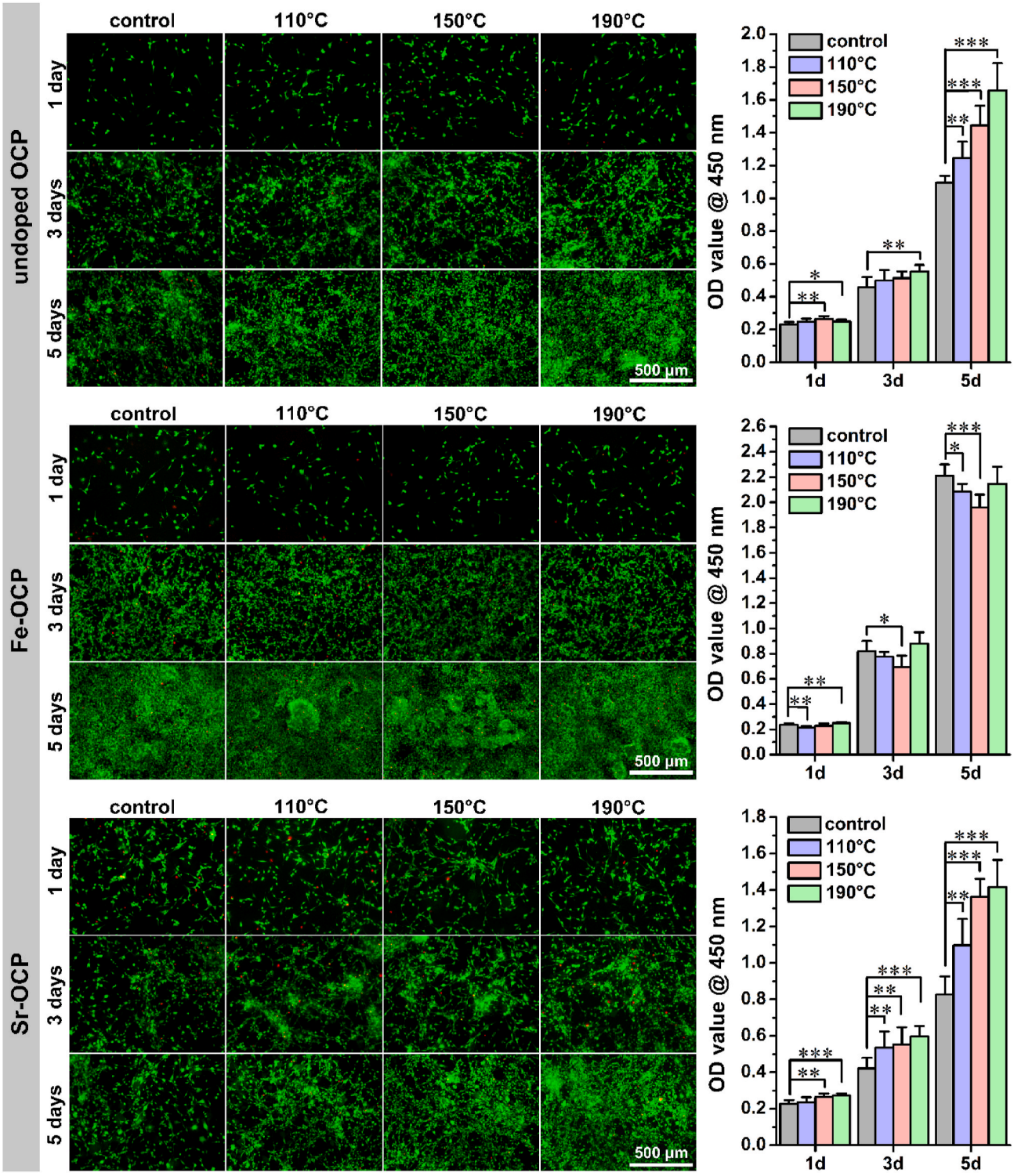

Fig. 8. The improved proliferation of BMSCs was determined as cultured with the heat-treated OCP samples. Live/dead staining fluorescence images and proliferation of BMSCs after co-cultured with heat-treated undoped OCP, Fe-OCP, and Sr-OCP for 1, 3, and 5 days, respectively. Scale bar = 500 μm. Data were presented as mean ± S.D., $n = 4$. * Heat-treated samples compared with the control sample. *$P < 0.05$, **$P < 0.01$, ***$P < 0.001$.

extent. Fe-OCP was relatively more unstable and easier to be activated into a positive state in favor of cellular adhesion and migration; Sr-OCP revealed more stable and was desensitized to the treatment. In addition, some divalent cations (e.g. Ca^{2+}, Mg^{2+}, and Mn^{2+}) can participate cellular adhesion process by interacting with integrins molecules through metal ion-dependent adhesion site (MIDAS), thus regulating the functions of integrins [42–44]. In general, most integrins have high-affinity Ca^{2+} sites, which are critical for integrin αβ heterodimer formation. Moreover, the intracellular Ca^{2+} fluxes can activate calpain, which regulates cluster formation of leucocyte integrins [40]. Herein, the expression of integrins is associated with the concentration of Ca^{2+} in the culture media. Heat treatment can lead to the dehydration of OCP

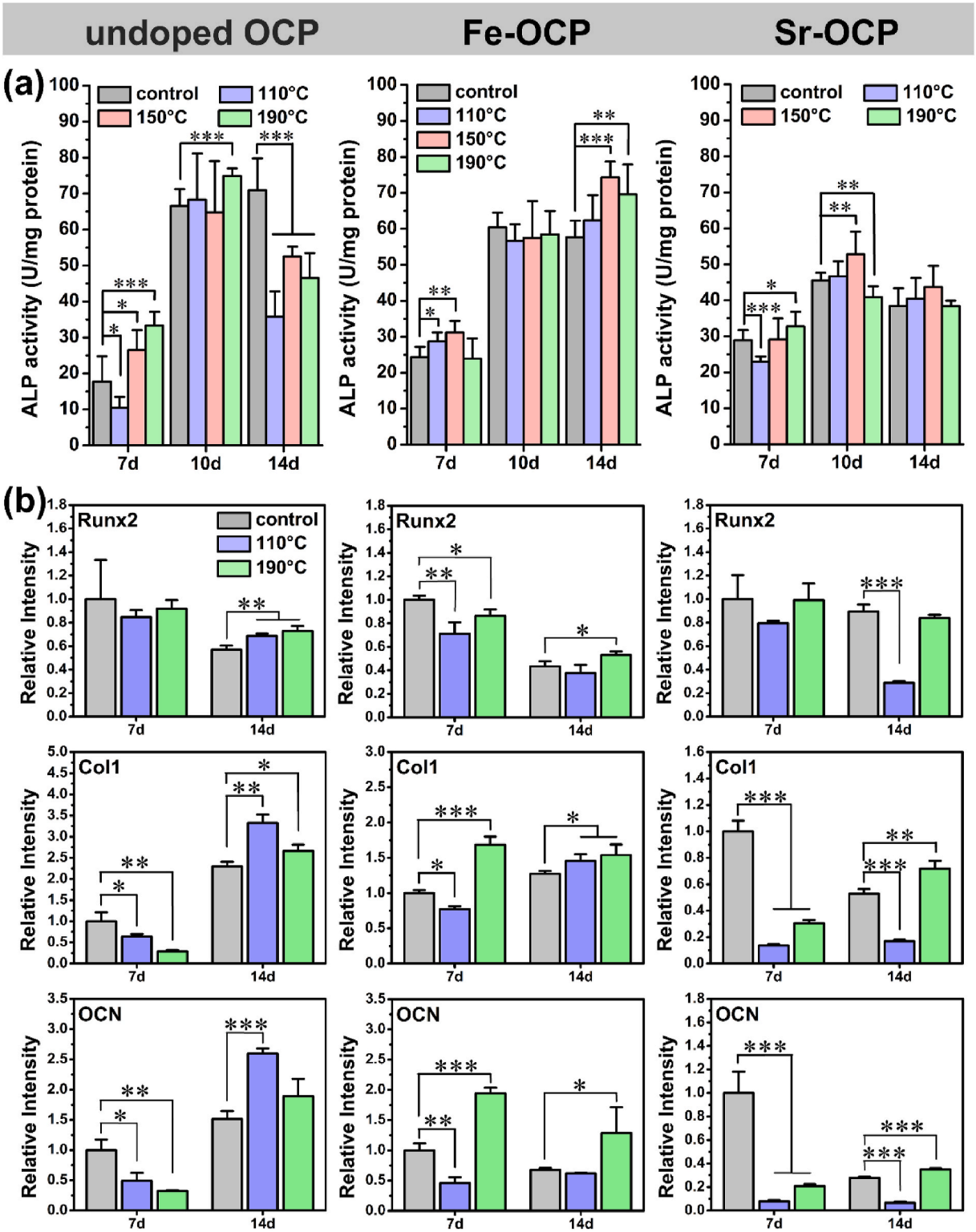

Fig. 9. The improved osteogenic differentiation of BMSCs was determined as cultured with the heat-treated OCP samples. ALP activity (a) and osteoblast-related gene expression (b) of BMSCs after co-cultured with heat-treated undoped OCP, Fe-OCP, and Sr-OCP for 7, 10 and 14 days, respectively. Data were presented as mean ± S.D., $n = 4$. * Heat-treated samples compared with the control sample. *$P < 0.05$, **$P < 0.01$, ***$P < 0.001$.

crystals with active surface layers, which released higher dose of Ca^{2+} and enhanced the integrin expression. It was inferred that more Ca^{2+} could be released from unstable heat-treated Fe-OCP and undoped OCP samples, and up-regulated the integrin expression; more stable Sr-OCP released relatively less Ca^{2+} and had slight effects on the integrin expression.

The live/dead staining fluorescence images and proliferation of mBMSCs after co-cultured with heat-treated undoped OCP, Fe-OCP, and Sr-OCP for different days are given in Fig. 8. The cells had good spreading shape and viability on all the OCP samples. As the culture time extended, the cells on all the OCP samples grew steadily, which indicated that all the OCP samples were nontoxic. Compared to the controls, the heat-treated undoped OCP and Sr-OCP samples were both beneficial to cellular viability in a temperature-dependent manner; the heat-treated Fe-OCP samples had no distinct difference in cellular viability. The quantitative results of cellular viability were determined by the CCK-8 method. The stable proliferation ability of mBMSCs was identified for all the OCP samples, which was consistent with the fluorescence observation. Compared to the relevant control, the heat-treated undoped OCP and Sr-OCP samples significantly promoted the proliferation of mBMSCs, and besides, the promotive effects enhanced with the increment of treatment temperature; the heat-treated Fe-OCP samples had a slight inhibition effect on the cellular proliferation. On the basis of these results, compared to the control, the promotive effects of heat-treated undoped OCP samples were attributed to their more active surface and higher dose of active ions (such as Ca^{2+}) in the early culture stage; for the heat-treated Fe-OCP samples, but excess Fe^{3+} release had an inhibitory effect on the cellular proliferation ability which neutralized the promotive effect of activated particle surface to some extent, and besides, the deposited nanosized ferric phosphates probably stripped out and gave birth to slight toxicity to cells after the heat treatment; the surface of the heat-treated Sr-OCP samples was relatively more stable (lower proteins adsorption), whilst the release of high dose of active ions (Ca^{2+} and Sr^{2+}) and its mildly activated surface synergistically promoted the cellular proliferation.

Fig. 9 shows the ALP activity and osteogenesis-related gene expression of mBMSCs after co-cultured with heat-treated undoped OCP, Fe-OCP, and Sr-OCP for different days. After 7 days of culture, compared to the control, all the heat-treated OCP samples up-regulated the ALP protein expression of mBMSCs. As the culture time prolonged to 10 days, the positive effects of these samples relatively decreased, whilst the heat-treated Fe-OCP samples even had no significant positive effects for the ALP activity. After 14 days, compared to the control, the heat-treated undoped OCP and Fe-OCP samples obviously down-regulated and up-regulated the ALP expression, respectively, whilst the heat-treated Sr-OCP samples had little impact on the ALP activity. The results showed that all the heat-treated OCP samples had notably promotive effects on the ALP activity and made the peak expression of this protein to different extent. In addition, the heat-treated Fe-OCP samples still played a positive role in the later culture stage. It was supposed that heat treatment could promote the ALP expression by improving the surface bioactivity of materials and the release of active ions. It should be noted that the positive effects of the heat-treated Fe-OCP samples were relatively weak in the early stage, which was probably due to the excessive release of Fe^{3+} at early stage and the free nanosized ferric phosphate. With the culture time prolonged, the concentration of Fe^{3+} gradually decreased, meanwhile the free nanoparticles were also gradually redeposited by mineralization or removed with the renewal of the culture media, leading to the gradual disappearance of the potential side effects, and thus the heat-treated Fe-OCP samples could still enhance the ALP activity of mBMSCs in the later stage. According to the results of mRNA expression of osteogenesis related genes, compared to the control, all the heat-treated undoped OCP and Sr-OCP samples as well as the Fe-OCP samples treated in low temperature (110 °C) down-regulated the mRNA expression levels of Runx2, Col1 and OCN, whilst the Fe-OCP samples treated in high temperature (190 °C) up-regulated the genes expression after 7 days of culture. As the culture time reached 14 days, compared to the control, all the heat-treated undoped OCP and Fe-OCP samples as well as the Sr-OCP samples treated in high temperature (190 °C) up-regulated the gene expression, whilst the Sr-OCP samples treated in low temperature (110 °C) down-regulated the gene expression. It was indicated that all the heat-treated OCP samples had inhibitory effect on the early mRNA expression of these genes, which could be due to the negative feedback regulation of osseous protein expressions [45,46]. Herein, these samples significantly promoted the advance expression of osteogenic proteins (such as ALP) and down-regulated the expression of osteogenesis related genes through the negative feedback system at the same time; in the later culture stage, as these samples stimulated osteogenic differentiation, the mRNA expression levels of osteogenesis related genes increased to a comparable or higher level compared to the control. In addition, OCP samples treated in higher temperature notably promoted the gene expression of mBMSCs compared to those in lower temperature, which was related to the corresponding higher surface activity and greater dose of released active ions.

3.4. Ions release in vitro of ion doped OCPs after treatment

The ions release behaviors of these OCP samples were tested via being immersed in the culture media. Tables 2 and 3 summarize the concentrations of Ca^{2+}, Fe^{3+}, and Sr^{2+} in the immersion media of heat-treated undoped OCP, Fe-OCP and Sr-OCP samples. After two days of immersion, the concentration of Ca^{2+} in the immersion media of all the heat-treated OCP samples was comparable with that of the control. As the immersion time went on, after six days, the concertation of Ca^{2+} in the immersion media of all the heat-treated OCP samples significantly higher than that of the control. Although the basic culture media (DMEM) could be used as immersion media to simulate the ionic environment during cell culture of OCP particles samples, at the same time, the cells also participated in the calcification process, which would promote the combination of calcium and phosphate as well as the further formation of calcified nodules, thus accelerating the exchange process of Ca^{2+}. In this regard, significant difference in [Ca^{2+}] between all the heat-treated OCP samples and their controls would manifest at an earlier culture stage, thus supporting the early active ions release behaviors during corresponding culture process. The behaviors of Ca^{2+} release also confirmed the stability difference between Fe-OCP and Sr-OCP. In addition, the concentrations of Fe^{3+} and Sr^{2+} released respectively from the heat-treated Fe-OCP and Sr-OCP samples were significantly higher than that of the controls during immersion process. It was also indicated that heat treatment could obviously improve the ionic exchange activity of Fe-OCP and Sr-OCP. In particular, the dose of Fe^{3+} released from the heat-treated Fe-OCP samples had reached a relatively higher level. As the cell culture went on, Fe^{3+} could be gradually fixed due to cellular metabolism, absorption, and calcification, and the corresponding concentration would be lower, but according to the results of Table 3, the concentration of Fe^{3+} might still be within the toxic range during cell culture.

Table 2
Ca^{2+} concentration of immersed media of heat-treated undoped OCP, Fe-OCP and Sr-OCP samples after immersion for 2 and 6 days, respectively.

Samples	Ca^{2+} concentration-2 days (mM)			Ca^{2+} concentration-6 days (mM)		
	control	110 °C	190 °C	control	110 °C	190 °C
undoped OCP	0.53 ± 0.01	0.51 ± 0.01	0.55 ± 0.01	0.73 ± 0.01	1.09 ± 0.01	2.22 ± 0.02
Fe-OCP	1.05 ± 0.01	1.31 ± 0.01	0.90 ± 0.01	1.89 ± 0.02	2.84 ± 0.01	2.38 ± 0.02
Sr-OCP	0.65 ± 0.01	0.58 ± 0.02	0.65 ± 0.01	0.75 ± 0.01	0.83 ± 0.01	0.92 ± 0.01

Table 3
Concentration of Fe^{3+} and Sr^{2+} released from heat-treated Fe-OCP and Sr-OCP samples after immersion for 2 and 6 days, respectively.

Samples	M^{n+} concentration-2 days (μM)[a]			M^{n+} concentration-6 days (μM)[a]		
	control	110 °C	190 °C	control	110 °C	190 °C
Fe-OCP	22.66 ± 0.25	27.10 ± 0.15	95.41 ± 0.50	72.06 ± 0.26	100.45 ± 0.86	133.06 ± 1.55
Sr-OCP	10.73 ± 0.08	10.50 ± 0.08	16.07 ± 0.05	2.72 ± 0.04	2.83 ± 0.05	5.74 ± 0.03

[a] M^{n+}. Represents Fe^{3+}. Or Sr^{2+}.

3.5. A brief mechanism for thermal-triggered activation of ion doped OCPs

Surface physicochemical properties and active ions release synergistically play important roles in the protein adsorption and cytological responses of the ion doped biomaterials. Here, the ion-doped OCP materials with different conversion degrees were successfully prepared by controlling the temperature (110–200 °C) of heat treatment. The effect of heat treatment on the protein adsorption and cytological responses of the ion doped OCP materials were preliminarily discussed from the aspects of surface activity and early ions release, as summarized in Table 4. It was of indicative that the heat-treated samples were beneficial to protein adsorption and cellular adhesion, spreading, proliferation and osteogenic differentiation compared to the untreated samples. Regarding material surface, OCP material still retains its main structural characteristics after heat treatment, but OCP crystals would generate defects and form a new phase called "collapsed OCP" after partial dehydration. The vacancy of hydrated layer makes the apatite layer be exposed and interact more actively with the medium, and thus activating the surface layer structure and increasing the specific surface area of the material to some extent. As immersed in culture medium, the material was more favorable for specific protein adsorption and subsequent cytological responses. With respect to ions release, heat treatment not only caused defects in the surface layer of materials but also promoted the ionic uptake and release in the material-medium interface region. In particular, the vacancy of hydrated layers of the "collapsed OCP" could provide more favorable and active channels for ionic exchange. The released active ions (e.g. Ca^{2+}, Fe^{3+}, and Sr^{2+}) had been proved to have good biocompatibility and could mediate the adhesion, proliferation and osteogenic differentiation of mBMSCs to different degrees [11,47,48]. Heat treatment mainly alerted the ionic exchange state of OCP material at the early stage of cell culture. With the extension of culture time, the ions release behaviors of "collapsed OCP" in the culture medium would gradually approach those of the untreated OCP, and the corresponding ionic exchange activity would gradually decrease. Therefore, the effect of active ions on the cellular behaviors of the heat-treated materials was mainly reflected in the first-half stage of cell culture.

Based on the two aspects above, for undoped OCP, active surface properties and early Ca^{2+} release synergistically promoted the protein adsorption and cellular adhesion, proliferation and osteogenic differentiation of the heat-treated samples. Fe-OCP was relatively unstable. The heat treatment could improve the surface activity, and at the same time, led to higher doses of early Fe^{3+} release and stripping out of partial nanosized particles, thus producing side effects on the proliferation in the early culture stage to some extent. As the culture time prolonged, the concentration of Fe^{3+} decreased and the free nanoparticles were removed, then the side effects gradually disappeared and the positive effects of heat treatment on the cellular behaviors gradually reflected in the later culture stage. By contrast, Sr-OCP was more stable. The heat treatment had no significant effects on its main characteristics. Nevertheless, the heat treatment could still activate the surface of Sr-OCP and promote its early release of the active ions (e.g. Sr^{2+}) to some extent, thus enhancing the proliferation and osteogenic differentiation of mBMSCs.

Table 4
Protein adsorption and cellular response of heat-treated undoped OCP, Fe-OCP and Sr-OCP samples as well as the correlated influencing factors[a].

Biological events	undoped OCP	Fe-OCP	Sr-OCP	Related factors	
				Surface properties	Early bioactive ions release
BSA adsorption	↑↑↑	↑↑↑	n.s.	✓	-
LSZ adsorption	↑↑↑	↓↓	n.s.	✓	-
Cellular adhesion area	n.s.	n.s.	↑	✓	-
Focal adhesion expression	↑	↑	↓↓	✓	-
Integrin α5β1 expression	↑↑↑	↑↑	n.s.	✓	✓
Cellular proliferation	↑↑	↓	↑↑↑	✓	✓
ALP activity	↑	↑↑	↑	✓	✓
Osteogenesis-related gene expression	First↓↓ Then↑↑	First↓↓ Then↑↑	First↓↓↓ Then↑↑	✓	✓

[a] ↑, ↑↑ and ↑↑↑ represent significant improvements ($P < 0.05$, 0.01, and 0.001, respectively); ↓, ↓↓ and ↓↓↓ represent significant inhibitions ($P < 0.05$, 0.01, and 0.001, respectively); n.s. Represents no significance..

Herein, the heat treatment had affected the surface physicochemical properties of the ion-doped OCP materials as well as their early release of active ions (Ca^{2+}, Fe^{3+} and Sr^{2+}), thereby changing the adsorption behaviors of specific proteins and regulating the subsequent cytological responses, including cellular adhesion, spreading, proliferation activity and osteogenic differentiation ability.

4. Conclusions

Octacalcium phosphate materials doped with different ions (Fe^{3+} and Sr^{2+}) were heat treated under air at different temperature (110–200 °C). The effects of the heat treatment on the phase, morphology, structure, surface properties, protein adsorption behaviors, ions release behaviors and cytological responses of the ion doped OCP materials were investigated comparatively. After heat treatment, the hydrated layer of OCP crystals gradually dehydrated, while the apatite layer did not change significantly. With the increase of temperature, plate-like OCP crystals gradually disintegrated into nanosized flake-like crystals with the increase of their surface areas. The obtained "collapsed OCP" crystals still retained the typical properties of OCP and had the potential of OCP-HA transformation. Compared to the control, Fe-OCP and Sr-OCP had lower and higher thermostability, respectively. This thermostable difference directly affected the physicochemical properties of material surface, especially the electronegative changes: as the temperature increased, the surface electronegativity of undoped OCP and Fe-OCP decreased gradually, while that of Sr-OCP remained almost no change, which further mediated the adsorption capacity of proteins (e.g. BSA and LSZ). The thermostable difference also altered the early active ions release behaviors of the ion doped OCP materials. Surface characteristics and early active ions release regulated cytological responses, mainly promoting the adhesion, spreading, proliferation and osteogenic differentiation of bone marrow mesenchymal stem cells to different degrees and stages.

Declaration of competing interest

None.

Acknowledgments

This work was supported by the National Natural Science Foundation

of China (Grant 31800791), the Natural Science Foundation of Guangdong Province (Grant 2018030310062), and the Fundamental Research Funds for the Central Universities (Grant 21620427).

Appendix A. Supplementary data

Supplementary data to this article can be found online at https://doi.org/10.1016/j.bioactmat.2020.10.025.

CRediT authorship contribution statement

Haishan Shi: Conceptualization, Writing - original draft, Methodology, Investigation, Validation, Funding acquisition, Software. **Xiaoling Ye:** Methodology, Investigation, Formal analysis. **Jing Zhang:** Methodology, Investigation. **Tingting Wu:** Data Curation, Visualization. **Tao Yu:** Validation. **Changren Zhou:** Validation. **Jiandong Ye:** Conceptualization, Funding acquisition, Supervision, Writing – review & editing.

References

[1] E. Boanini, M. Gazzano, A. Bigi, Ionic substitutions in calcium phosphates synthesized at low temperature, Acta Biomater. 6 (6) (2010) 1882–1894, https://doi.org/10.1016/j.actbio.2009.12.041.

[2] M. Šupová, Substituted hydroxyapatites for biomedical applications: a review, Ceram. Int. 41 (8) (2015) 9203–9231, https://doi.org/10.1016/j.ceramint.2015.03.316.

[3] A. Bigi, E. Boanini, M. Gazzano, 7 - ion substitution in biological and synthetic apatites, in: C. Aparicio, M.-P. Ginebra (Eds.), Biomineralization and Biomaterials, Woodhead Publishing, Boston, 2016, pp. 235–266.

[4] S. Gomes, C. Vichery, S. Descamps, H. Martinez, A. Kaur, A. Jacobs, J.-M. Nedelec, G. Renaudin, Cu-doping of calcium phosphate bioceramics: from mechanism to the control of cytotoxicity, Acta Biomater. 65 (2018) 462–474, https://doi.org/10.1016/j.actbio.2017.10.028.

[5] Y. Su, I. Cockerill, Y. Wang, Y.-X. Qin, L. Chang, Y. Zheng, D. Zhu, Zinc-based biomaterials for regeneration and therapy, trends, Biotechnol. 37 (4) (2019) 428–441, https://doi.org/10.1016/j.tibtech.2018.10.009.

[6] Y. Honda, T. Anada, S. Morimoto, Y. Shiwaku, O. Suzuki, Effect of Zn^{2+} on the physicochemical characteristics of octacalcium phosphate and its hydrolysis into apatitic phases, Cryst. Growth Des. 11 (5) (2011) 1462–1468, https://doi.org/10.1021/cg1009835.

[7] Y. Qiao, W. Zhang, P. Tian, F. Meng, H. Zhu, X. Jiang, X. Liu, P.K. Chu, Stimulation of bone growth following zinc incorporation into biomaterials, Biomaterials 35 (25) (2014) 6882–6897, https://doi.org/10.1016/j.biomaterials.2014.04.101.

[8] V. Graziani, M. Fosca, A.A. Egorov, Y.V. Zobkov, A.Y. Fedotov, A.E. Baranchikov, M. Ortenzi, R. Caminiti, V.S. Komlev, J.V. Rau, Zinc-releasing calcium phosphate cements for bone substitute materials, Ceram. Int. 42 (15) (2016) 17310–17316, https://doi.org/10.1016/j.ceramint.2016.08.027.

[9] X. Xu, N. Wang, M. Wu, J. Wang, D. Wang, Z. Chen, J. Xie, C. Ding, J. Li, Programmed antibacterial and mineralization therapy for dental caries based on zinc-substituted hydroxyapatite/alendronate- grafted polyacrylic acid hybrid material, Colloids Surf., B 194 (2020) 111206, https://doi.org/10.1016/j.colsurfb.2020.111206.

[10] M.E. Conrad, J.N. Umbreit, Pathways of iron absorption, blood cell, Mol. Dis. 29 (3) (2002) 336–355, https://doi.org/10.1006/bcmd.2002.0564.

[11] J. Zhang, H.S. Shi, J.Q. Liu, T. Yu, Z.H. Shen, J.D. Ye, Good hydration and cell-biological performances of superparamagnetic calcium phosphate cement with concentration-dependent osteogenesis and angiogenesis induced by ferric iron, J. Mater. Chem. B 3 (45) (2015) 8782–8795, https://doi.org/10.1039/C5TB01440A.

[12] H. Shi, S. Yang, S. Zeng, X. Liu, J. Zhang, J. Zhang, T. Wu, X. Ye, T. Yu, C. Zhou, J. Ye, Enhanced angiogenesis of biodegradable iron-doped octacalcium phosphate/poly(lactic-co-glycolic acid) scaffold for potential cancerous bone regeneration, Appl. Mater. Today 15 (2019) 100–114, https://doi.org/10.1016/j.apmt.2019.01.002.

[13] H.-C. Wu, T.-W. Wang, J.-S. Sun, W.-H. Wang, F.-H. Lin, A novel biomagnetic nanoparticle based on hydroxyapatite, Nanotechnology 18 (16) (2007) 165601, https://doi.org/10.1088/0957-4484/18/16/165601.

[14] Q. Chang, D.L. Chen, H.Q. Ru, X.Y. Yue, L. Yu, C.P. Zhang, Toughening mechanisms in iron-containing hydroxyapatite/titanium composites, Biomaterials 31 (7) (2010) 1493–1501, https://doi.org/10.1016/j.biomaterials.2009.11.046.

[15] M. Schumacher, M. Gelinsky, Strontium modified calcium phosphate cements – approaches towards targeted stimulation of bone turnover, J. Mater. Chem. B 3 (23) (2015) 4626–4640, https://doi.org/10.1039/c5tb00654f.

[16] C.T. Wong, W.W. Lu, W.K. Chan, K.M. Cheung, K.D. Luk, D.S. Lu, A.B. Rabie, L. F. Deng, J.C. Leong, In Vivo cancellous bone remodeling on a strontium-containing hydroxyapatite (Sr-HA) bioactive cement, J. Biomed. Mater. Res. A 68 (3) (2004) 513–521, https://doi.org/10.1002/jbm.a.20089.

[17] H.S. Shi, F.P. He, J.D. Ye, Synthesis and structure of iron- and strontium-substituted octacalcium phosphate: effects of ionic charge and radius, J. Mater. Chem. B 4 (9) (2016) 1712–1719, https://doi.org/10.1039/c5tb02247a.

[18] O. Suzuki, Octacalcium phosphate: osteoconductivity and crystal chemistry, Acta Biomater. 6 (9) (2010) 3379–3387, https://doi.org/10.1016/j.actbio.2010.04.002.

[19] W. Pompe, H. Worch, W.J.E.M. Habraken, P. Simon, R.D. Kniep, H. Ehrlich, P. Paufler, Octacalcium phosphate – a metastable mineral phase controls the evolution of scaffold forming proteins, J. Mater. Chem. B 3 (26) (2015) 5318–5329, https://doi.org/10.1039/C5TB00673B.

[20] S. Kajiyama, T. Sakamoto, M. Inoue, T. Nishimura, T. Yokoi, C. Ohtsuki, T. Kato, Rapid and topotactic transformation from octacalcium phosphate to hydroxyapatite (HAP): a new approach to self- organization of free-standing thin-film HAP-based nanohybrids, CrystEngComm 18 (43) (2016) 8388–8395, https://doi.org/10.1039/C6CE01336H.

[21] A. Carino, C. Ludwig, A. Cervellino, E. Müller, A. Testino, Formation and transformation of calcium phosphate phases under biologically relevant conditions: experiments and modelling, Acta Biomater. 74 (2018) 478–488, https://doi.org/10.1016/j.actbio.2018.05.027.

[22] O. Suzuki, S. Kamakura, T. Katagiri, M. Nakamura, B. Zhao, Y. Honda, R. Kamijo, Bone formation enhanced by implanted octacalcium phosphate involving conversion into Ca-deficient hydroxyapatite, Biomaterials 27 (13) (2006) 2671–2781, https://doi.org/10.1016/j.biomaterials.2005.12.004.

[23] O. Suzuki, S. Kamakura, T. Katagiri, Surface chemistry and biological responses to synthetic octacalcium phosphate, J. Biomed. Mater. Res. B 77 (1) (2006) 201–212, https://doi.org/10.1002/jbm.b.30407.

[24] O. Suzuki, H. Yagishita, M. Yamazaki, T. Aoba, Adsorption of bovine serum albumin onto octacalcium phosphate and its hydrolyzates, Cell Mater. 5 (1995) 45–54.

[25] X. Yang, X. Gao, Y. Gan, C. Gao, X. Zhang, K. Ting, B.M. Wu, Z. Gou, Facile synthesis of octacalcium phosphate nanobelts: growth mechanism and surface adsorption properties, J. Phys. Chem. C 114 (14) (2010) 6265–6271, https://doi.org/10.1021/jp911576f.

[26] Y. Shiwaku, T. Anada, H. Yamazaki, Y. Honda, S. Morimoto, K. Sasaki, O. Suzuki, Structural, morphological and surface characteristics of two types of octacalcium phosphate-derived fluoride-containing apatitic calcium phosphates, Acta Biomater. 8 (12) (2012) 4417–4425, https://doi.org/10.1016/j.actbio.2012.07.041.

[27] E. Boanini, P. Torricelli, M. Gazzano, M. Fini, A. Bigi, Crystalline calcium alendronate obtained by octacalcium phosphate digestion: a new chance for local treatment of bone loss diseases? Adv. Mater. 25 (33) (2013) 4605–4611, https://doi.org/10.1002/adma.201301129.

[28] H. Imaizumi, M. Sakurai, O. Kashimoto, T. Kikawa, O. Suzuki, Comparative study on osteoconductivity by synthetic octacalcium phosphate and sintered hydroxyapatite in rabbit bone marrow, Calcif. Tissue Int. 78 (1) (2006) 45–54, https://doi.org/10.1007/s00223-005-0170-0.

[29] H. Kaneko, J. Kamiie, H. Kawakami, T. Anada, Y. Honda, N. Shiraishi, S. Kamakura, T. Terasaki, H. Shimauchi, O. Suzuki, Proteome analysis of rat serum proteins adsorbed onto synthetic octacalcium phosphate crystals, Anal. Biochem. 418 (2) (2011) 276–285, https://doi.org/10.1016/j.ab.2011.07.022.

[30] S. Kamakura, K. Sasaki, Y. Honda, T. Anada, T. Kawai, K. Matsui, S. Echigo, O. Suzuki, Stability of regenerated bone by octacalcium phosphate (OCP) combined with collagen, Key Eng. Mater. 330– 332 (2007) 1315–1318. https://doi.org/10.4028/www.scientific.net/KEM.330-332.1315.

[31] T. Kawai, S. Echigo, K. Matsui, Y. Tanuma, T. Takahashi, O. Suzuki, S. Kamakura, First clinical application of octacalcium phosphate collagen composite in human bone defect, Tissue Eng. 20 (7–8) (2014) 1336–1341, https://doi.org/10.1089/ten.tea.2013.0508.

[32] T. Kawai, Y. Tanuma, K. Matsui, O. Suzuki, T. Takahashi, S. Kamakura, Clinical safety and efficacy of implantation of octacalcium phosphate collagen composites in tooth extraction sockets and cyst holes, J. Tissue Eng. 7 (2016), https://doi.org/10.1177/2041731416670770.

[33] A. Bigi, G. Cojazzi, M. Gazzano, A. Ripamonti, N. Roveri, Thermal conversion of octacalcium phosphate into hydroxyapatite, J. Inorg. Biochem. 40 (4) (1990) 293–299, https://doi.org/10.1016/0162-0134(90)80063-4.

[34] E. Boanini, M. Gazzano, K. Rubini, A. Bigi, Collapsed octacalcium phosphate stabilized by ionic substitutions, cryst, Growth Des 10 (8) (2010) 3612–3617, https://doi.org/10.1021/Cg100494f.

[35] K. Matsunaga, H. Murata, Strontium substitution in bioactive calcium phosphates: a first- principles study, J. Phys. Chem. B 113 (11) (2009) 3584–3589, https://doi.org/10.1021/jp808713m.

[36] W.E. Brown, J.P. Smith, J.R. Lehr, A.W. Frazier, Octacalcium phosphate and hydroxyapatite: crystallographic and chemical relations between octacalcium phosphate and hydroxyapatite, Nature 196 (4859) (1962) 1050–1055, https://doi.org/10.1038/1961050a0.

[37] M. van der Veen, W. Norde, M.C. Stuart, Electrostatic interactions in protein adsorption probed by comparing lysozyme and succinylated lysozyme, Colloids Surf., B 35 (1) (2004) 33–40, https://doi.org/10.1016/j.colsurfb.2004.02.005.

[38] R.A. Latour, G.L. Bowlin, G. Wnek, Biomaterials: protein–surface interactions, Encyclopedia of Biomaterials and Biomedical Engineering 270 (2005), https://doi.org/10.1081/E-EBBE-120041856.

[39] T. Kobayashi, S. Nakamura, K. Yamashita, Enhanced osteobonding by negative surface charges of electrically polarized hydroxyapatite, J. Biomed. Mater. Res. 57 (4) (2001) 477–484, https://doi.org/10.1002/1097-4636(20011215)57:4<477::AID-JBM1193>3.0.CO.

[40] E.M. Burke, G.H. Nancollas, Relation of lattice ion solution composition to octacalcium phosphate dissolution kinetics, Colloid. Surface. A 150 (1–3) (1999) 151–160, https://doi.org/10.1016/S0927-7757(98)00846-2.

[41] X.D. Zhu, H.S. Fan, C.Y. Zhao, T. Ikoma, M. Tanaka, J.Y. Chen, X.D. Zhang, Bovine serum albumin adsorption on hydroxyapatite. And Biphasic Calcium Phosphate and the Correlation with Zeta Potentials and Wettability, Key Eng. Mater., Trans. Tech. Publ., 2006, pp. 73–76. https://doi.org/10.4028/www.scientific.net/KEM.309-311.73.

[42] J.J. Grzesiak, G.E. Davis, D. Kirchhofer, M.D. Pierschbacher, Regulation of alpha 2 beta 1-mediated fibroblast migration on type I collagen by shifts in the concentrations of extracellular Mg^{2+} and Ca^{2+}, J. Cell Biol. 117 (5) (1992) 1109–1117, https://doi.org/10.1083/jcb.117.5.1109.

[43] B. Leitinger, A. McDowall, P. Stanley, N. Hogg, The regulation of integrin function by Ca^{2+}, BBA- Mol. Cell Res. 1498 (2–3) (2000) 91–98, https://doi.org/10.1016/S0167-4889(00)00086-0.

[44] J.-L. Banères, F. Roquet, A. Martin, J. Parello, A minimized human integrin α5β1 that retains ligand recognition, J. Biol. Chem. 275 (8) (2000) 5888–5903, https://doi.org/10.1074/jbc.275.8.5888.

[45] G.S. Stein, J.B. Lian, T.A. Owen, Relationship of cell growth to the regulation of tissue-specific gene expression during osteoblast differentiation, Faseb. J. 4 (13) (1990) 3111–3123, https://doi.org/10.1096/fasebj.4.13.2210157.

[46] D.M. Bader, S. Wilkening, G. Lin, M.M. Tekkedil, K. Dietrich, L.M. Steinmetz, J. Gagneur, Negative feedback buffers effects of regulatory variants, Mol. Syst. Biol. 11 (1) (2015) 785, https://doi.org/10.15252/msb.20145844.

[47] S. Peng, G. Zhou, K.D. Luk, K.M. Cheung, Z. Li, W.M. Lam, Z. Zhou, W.W. Lu, Strontium promotes osteogenic differentiation of mesenchymal stem cells through the Ras/MAPK signaling pathway, Cell. Physiol. Biochem. 23 (1–3) (2009) 165–174, https://doi.org/10.1159/000204105.

[48] H. Shi, X. Ye, T. Wu, J. Zhang, J. Ye, Regulating the physicochemical and biological properties in vitro of octacalcium phosphate by substitution with strontium in a large doping range, Mater. Today Chem. (2017) 81–91, https://doi.org/10.1016/j.mtchem.2017.07.003.